1-D and 2-D Loss-Measuring Methods: Optimized Setup Design, Advanced Testing, and Results

1D and 2D loss measuring methods: optimized setup design, advanced testing, results.

O. de la Barrière[1a], C. Appino[2], C. Ragusa[3], F. Fiorillo[2], M. LoBue[1], F. Mazaleyrat[1]

[1]Laboratoire SATIE, CNRS - ENS Cachan, F-94230 Cachan, France
[2]Nanoscience and Materials Division, INRiM, Turin, Italy
[3]Energy Department, Politecnico di Torino, Torino 10129, Italy

Accurate measurements of magnetic losses in laminations are a prerequisite for their theoretical assessment, as well as for satisfying calculations of energy dissipation in engineering systems. The standardized and universally applied measurement method, used as a reference for the definition of the material quality in the specification standards, is based on the Epstein test frame magnetizer. Its success relies on the reproducibility of the performed measurements. Its limitations come, on the one hand, from cumbersome sample preparation and, on the other hand, from a certain divergence of the measured loss figures from the true loss figures. Similar systematic differences between measured and true loss values are also observed with the standard Single Sheet Tester method. In both cases, measurements under bi-dimensional induction are or cannot be envisaged. The design of new measurement setups and magnetizers overcoming the drawbacks of the Epstein and Single Sheet Tester methods and possibly becoming recognized Standards in the future is welcome, but challenging. This paper is devoted to a comprehensive discussion of the state of the art in the alternating and two-dimensional measurements of energy losses in soft magnetic materials for electrical applications. We will summarize, in particular, measuring solutions proposed in the current literature and we will discuss in detail recent developments achieved in the authors' labs regarding 1D measurements with compensated permeameters and 2D measurements at high inductions and high frequencies.

***Index Terms*—Magnetic losses, Magnetic measurements, Permeameter, Two-dimensional magnetization.**

I. Introduction

Electrical machine designers are nowadays facing difficult challenges. For example, the rapid growth of demand in embedded applications, such as hybrid/electric cars [*1*], require the design of very compact actuators [*2*]. In this context, materials are often used at the limit of their thermal viability, so realistic designs impose accurate loss calculations. Should these be based on magnetic loss models or should they rely on empirical formulations, there is no alternative to precise loss measurements [*3*]. The standard measurement methods, based on the use of the Epstein frame [*4*][*5*] or the Single Sheet Testing (SST) magnetizer with flux closing yokes [*6*], offer good reproducibility, as verified by a number of international comparisons [*7*][*8*]. They are therefore assumed as reference methods for the definition of the material quality in the specification standards. However, both Epstein and SST methods generate systematic contributions to the measurement uncertainty [*9*] and the obtained loss figures can be appreciably different from the "true" loss values, those provided by accurate local measurements of the effective magnetic field strength and the flux density [*8*] [*9*][*10*]. An example concerning non-oriented and grain-oriented Fe-Si steel sheets is shown in Fig. 1. It is to remark that the Epstein strip samples require tedious preparation, including relief of cutting stresses. In addition, Epstein and SST methods are hardly compatible with two-dimensional induction loci [*11*], a typical working regime in electrical machine cores. It turns out that the losses due to the two components of the flux density locus are often computed separately and summed up, as if they were independent alternating magnetization processes [*12*]. This procedure is clearly inaccurate, especially at high flux density values, where the hysteresis loss, always increasing with alternating flux, tends to vanish under circular flux density on approaching the saturation. No measuring standards exist for rotating flux density, though many research efforts have been devoted to the development of 2D induction setups. Different solutions have actually been envisaged for the 2D magnetizer, like the horizontal [*13*][*14*][*15*] and vertical [*16*] [*17*] cross-shaped yokes and the three-phase yoke with either hexagonal [*18*] or circular [*19*] samples. In the latter case, flux density values up to 1.85 T could be reached, with maximum frequency around a few hundred Hz, under both alternating and rotational flux [*20*]. These limiting values of flux density and frequency should however be overcome, in order to meet the conditions of modern electrical machine cores, often attaining the saturated state and working at kHz frequencies.

In this paper, present-day developments in alternating and two-dimensional measurements of magnetic losses will be discussed, with emphasis on recent progress made in the authors labs (SATIE, INRIM, Politecnico di Torino), overcoming the previous limits. Two main points are addressed:

[a] Corresponding author, e-mail : barriere@satie.ens-cachan.fr

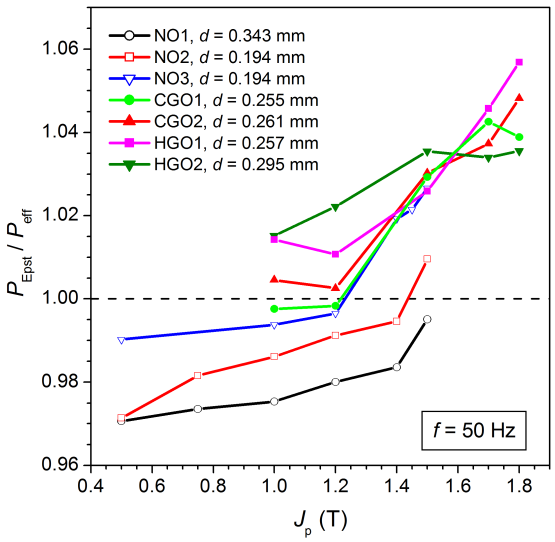

Fig. 1. Ratio of the Epstein to the effective ("true")power loss figure P_{Epst}/P_{eff} at 50 Hz measured in different types of non-oriented and grain-oriented steel sheets. $P_{eff}(J_p)$ is obtained by precise local measurement of magnetic field strength and flux density.

- *Alternating flux.* The Single Sheet Tester will be specifically considered, because it allows for a flexible approach to material testing. SST measurements may show slightly inferior reproducibility with respect to the Epstein measurements [*8*], since the quality of the yoke, its losses, and the reluctance of the sheet-yoke contact region can play a role. A novel approach to the SST method [*21*], where the potential drop occurring in different parts of the magnetic circuit is automatically compensated by means of a feedback system, will be here highlighted.
- *Two-dimensional flux*. The ambitious objective of reaching very high flux density values and high frequencies under controlled 2D fluxes and measuring the associated loss figures has been addressed in recent times (see for example [*22*] or [*23*]). To this end, two setups have been realized, those employ circular samples and three-phase magnetizers. One setup has been optimized to reach the kilohertz range, the other for approaching the magnetic saturation. Both fieldmetric and thermometric loss measurement methods have been applied.

Significant results for rotating and alternating flux densities will be discussed in the following.

II. Loss Measurements under Alternating Magnetic Field Strength

A. Standard methods

The characterization of soft magnetic materials under alternating magnetic field strengths is well standardized, but room exists for improved and wider-range measurements. We summarize here the main features of the present-day measuring approaches.

1) Toroidal sample.

Measurements in soft magnets can seldom be done on open samples, because demagnetizing fields are large and generally non-uniform. But a perfectly closed magnetic circuit, free of macroscopic demagnetizing effects, can ideally be achieved only using toroidal samples with uniformly distributed primary winding [*9*]. This approach is widely used with bulk materials, such as ferrites and Soft Magnetic Composites (SMC) [*24*], and described in the standards [*25*] [*26*]. It can be used with materials in sheet or ribbon form, either tapewound or made by stacking punched rings, possibly after release of bending or residual stresses by annealing. Problems nevertheless arise, because, with the length of the circumferential magnetic field strength lines depending on the inverse of their diameter, a ratio between outer and inner diameter $D_o / D_i < 1.1$ is prescribed, a condition sometimes difficult to fulfill [*27*]. Limitations may also appear regarding the maximum number of turns, that is, the maximum applicable magnetic field strength value .

2) Epstein frame

The Epstein frame is adopted in the IEC60404-2 standard for measurements on magnetic sheets. These are cut as strip samples (length 300 mm, width 30 mm), stacked and arranged to form a square magnetic circuit with double lapped joints. The related IEC standards cover the frequency ranges DC $\leq f \leq$ 400 Hz (700-turn primary and secondary windings) [*4*] and 400 Hz $\leq f \leq$ 10 kHz (200-turn windings) [*5*]. A fixed magnetic path length l_m = 0.94 m is assumed, independently of material, flux density level, and frequency. Non-oriented (NO) alloys are tested by stacking alternate layers of strips cut along the rolling direction (RD) and the transverse direction (TD), in order to cope with the non-negligible anisotropic response of these materials. The properties of the grain-oriented (GO) alloys are instead measured on strips cut along the rolling direction.

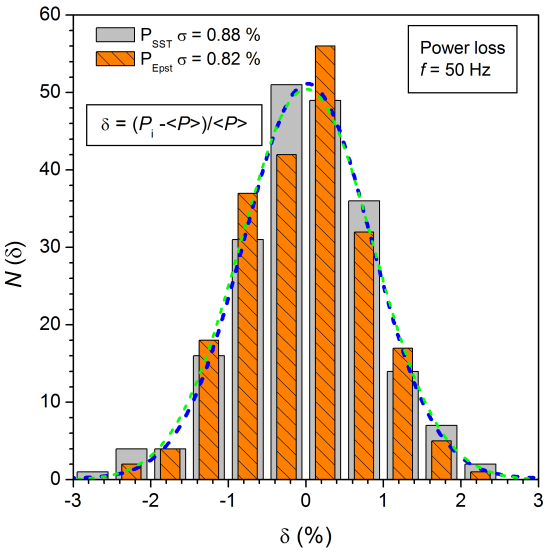

Fig. 2. Dispersion around the reference value of the laboratories best estimate of the power loss measured by the Epstein (P_{Epst}) and the SST (P_{SST}) methods in GO sheets. The related intercomparison is discussed in [*8*]. $N(\delta)$ is the number of laboratories whose best estimate P_i deviates from the reference value $\langle P \rangle$ by the relative quantity $\delta = (P_i - \langle P \rangle)/\langle P \rangle$. The dashed lines are best fits of the experimental distribution by a Gaussian function. The relative standard deviation σ associated with the measurements is lower than 1 %.

A main advantage of the Epstein frame is the good reproducibility of the measurements, as verified by international comparisons [*7*] [*8*]. Fig. 2 provides an example of dispersion of results concerning the measurement of the 50 Hz power losses P_{Epst} and P_{SST} in GO steels, as obtained by eleven different laboratories belonging to academia and

industry [*8*]. The statistical analysis is made on 212 loss figures (after excluding few outliers) provided by the participating laboratories. The data concern five different GO steel types, tested at the peak polarization values J_p = 1.3, 1.5, 1.5, 1.7 T. The global relative standard deviation of the measured P_{Epst} values around the best estimate <*P*> is σ_{Epst} = 0. 82 % (σ_{SST} = 0. 88 %). Since the very same samples are tested and the stacking procedure is strictly defined, the dispersion among the laboratories best estimates is attributed to the performance and the calibration features of the measuring setups.

The imperfections (capacitive effects, leakage flux…) of the Epstein frame that can affect the loss measurements have been discussed by Brugel, et al. [*28*]. By assuming a defined magnetic path length l_m = 0.94 m one makes an obvious oversimplification, inevitably conflicting with the evolution of the flux patterns in the magnetic circuit with *f*, J_p, and the material type. We can nevertheless lump the objective complexity of such an evolution into an effective magnetic path length $l_{eff}(J_p)$, associated with the effective (true) power loss value P_{eff}, which relates then to l_m and the standard Epstein loss figure P_{Epst} according to

$$P_{\mathrm{eff}}(J_\mathrm{p}) = P_{\mathrm{epst}}(J_\mathrm{p}) \cdot l_\mathrm{m} / l_{\mathrm{eff}}(J_\mathrm{p}) \qquad (1)$$

The results in Fig. 1 are therefore understood in terms of monotonical increase of $l_{eff}(J_p)$ with J_p, both in NO and GO sheets.

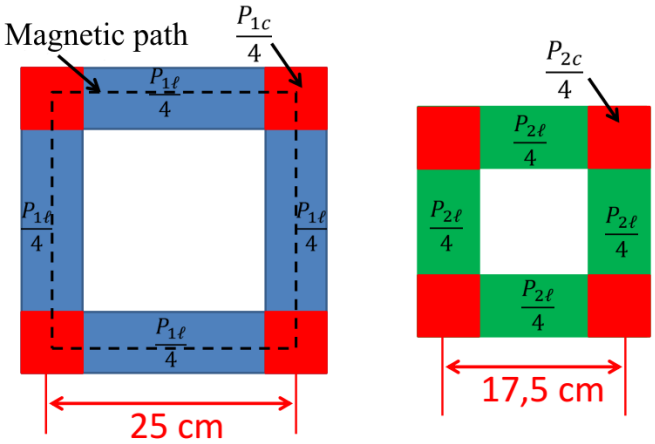

Fig. 3. Two Epstein frames with different limb lengths have been employed to determine the effective magnetic path length $l_{eff}(J_p)$. Its derivation relies on the assumption that the power loss in the corner regions is independent of the frame size [*29*][*30*].

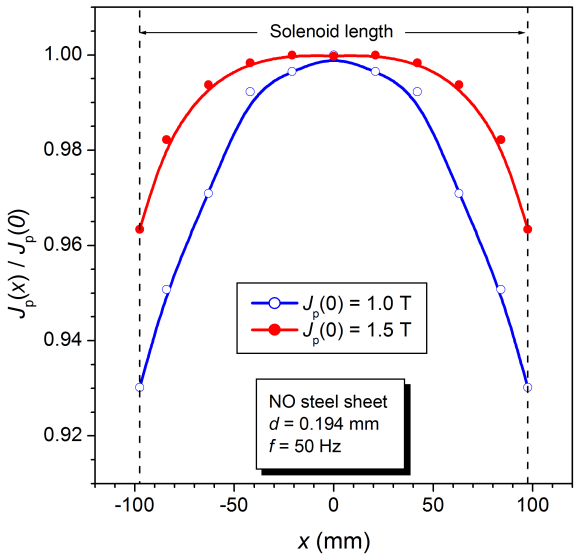

Fig. 4. Reduced value $J_p(x)$ / $J_p(0)$ of the peak polarization in NO Fe-Si strip samples across the limb length l_0 = 195 mm (the length covered by the windings, with center at *x* = 0) of a standard Epstein frame. $J_p(x)$ is measured by means of a localized pickup coil, collinear with a narrow *H*-coil, allowing for simultaneous measurement of P_{Epst} and the local power loss $P_{eff}(x)$ [*10*].

The problem of justifying from a physical viewpoint the behavior of $l_{eff}(J_p)$ has been considered both through Finite Element calculations [*31*] and by *ad hoc* experiments. Ahlers and Sievert compared Epstein frame and single strip measurements and justified the found behavior of l_{eff} by expressing it as $l_{eff} = l_0 + (\mu_l/2\mu_c)\cdot l_c$, the sum of the legs length l_0 and a portion of the corners length l_c depending on the ratio of the leg to corner permeabilities μ_l and μ_c [*32*]. A natural approach to the determination of l_{eff} consists in assuming, as done in [*29*][*30*], that the total power loss Π_{Epst} measured with the Epstein frame can be decomposed in two terms, one (Π_{l0}) in the limbs, the portion of the frame of length l_0 covered by the windings, the other (Π_c) in the corners . The somewhat crude assumption is made in [*29*][*30*] that Π_c is independent of the frame size and the polarization is uniform in the limbs, thereby making Π_{l0} proportional to the limbs length. By comparing the loss figures obtained with two frames having different limb length, the two loss contributions are discriminated. A standard 25 cm frame and a reduced 17.5 cm frame have been considered in [*29*][*30*], as sketched in Fig. 3. If the total loss values Π_{Epst1} and Π_{Epst2} are measured in the larger and smaller frame, respectively, we can write

$$\begin{aligned} \Pi_{\mathrm{Epst1}}(J_\mathrm{p}) &= \Pi_\mathrm{c}(J_\mathrm{p}) + \Pi_{l1}(J_\mathrm{p}) \\ \Pi_{\mathrm{Epst2}}(J_\mathrm{p}) &= \Pi_\mathrm{c}(J_\mathrm{p}) + \Pi_{l2}(J_\mathrm{p}) \end{aligned} \qquad (2)$$

and we obtain $\Pi_{\mathrm{Epst1}}(J_\mathrm{p}) - \Pi_{\mathrm{Epst2}}(J_\mathrm{p}) = \Pi_{l1}(J_\mathrm{p}) - \Pi_{l2}(J_\mathrm{p})$. In this way, the loss per unit volume $P_{l0}\left(J_p\right) = \Pi_{l0}\left(\mathrm{J}_p\right) / \mathrm{Al}_p$, where *A* is the cross-sectional area of the sample, is obtained and the effective magnetic path length is retrieved from (1). A similar approach has been followed by the authors of [*33*], who used three Epstein frames. However, small deviations from uniformity of the magnetization inside the Epstein legs inevitably occur, impairing to some extent this conclusion. A detailed investigation on the evolution of effective magnetic field strength and polarization along the limbs, performed by

means of localized *H*- and *B*-coils, on non-oriented, conventional grain-oriented (CGO) and high-permeability grain-oriented (HGO) sheets, actually shows non-negligible decrease of the polarization value $J_p(x)$ across the limb length from center to corners in all materials [*10*]. Fig. 4 provides an example of decrease of $J_p(x)$ across the Epstein limbs in NO Fe-Si strips. If $J_{0p} = \frac{1}{l_0}\int_{-l_0/2}^{l_0/2} J_p(x)\,dx$ is the peak polarization value measured by the secondary Epstein winding, the conventional power loss figure is obtained as

$$P_{epst}(J_{0p}) = \frac{1}{T}\cdot\frac{N_H}{l_m}\int_0^T i_H(t)\cdot J_{0p}\,\omega\cos(\omega t)\,dt \qquad (3)$$

where $i_H(t)$ is the magnetizing current. The corresponding true power loss is given by the average value of the locally measured power loss $P_{eff}(x)$ across the length l_0

$$P_{eff}(J_{0p}) = \frac{1}{l_0}\int_{-l_0/2}^{l_0/2} P_{eff}(J_p(x))\,dx \qquad (4)$$

The power loss increases more than linearly with J_p, according to the power law $P_{eff}(J_p) \propto J_p^n$, with n, in turn, a function of J_p. $P_{eff}(J_{0p})$ becomes then dependent on the profile of $J_p(x)$ and the effective magnetic path length will consequently evolve with J_{0p} according to the equation

$$l_{eff}(J_{0p}) = l_m\cdot\frac{P_{epst}(J_{0p})}{P_{eff}(J_{0p})} \qquad (5)$$

l_{eff} is found to be an increasing function of J_{0p} in all the previous NO (0.5 T ≤ J_{0p} ≤ 1.5 T) and GO (1.0 T ≤ J_{0p} ≤ 1.8 T) alloys. It approximately ranges between 0.92 m and 0.98 m. Such an increase is understood and calculated in terms of $J_p(x)$ profile and $n(J_p)$ behavior [*10*].

3) Single Sheet Tester (SST)

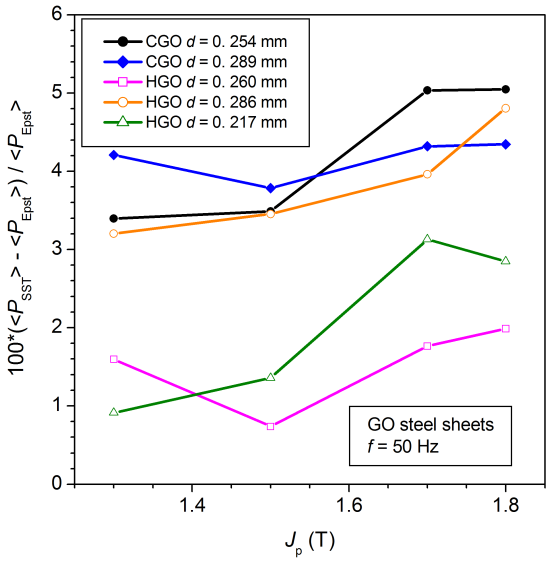

Fig. 5. The loss figure measured with the SST method P_{SST} (IEC60404-3) in CGO and HGO alloys is higher (~1 % - ~5 %) than the same quantity (P_{Epst}) measured using the Epstein frame (IEC60404-2) (adapted from [*8*], where the symbol <.> means the mean result between the different laboratories of the international comparison).

The SST standard IEC 60404-3 is based on the use of a single sheet of length 500 mm and width ranging between 300 mm and 500 mm, inserted between the pole faces of a double-C 500 mm × 500 mm flux-closing laminated yoke, made of GO Fe-Si sheets [*6*][*34*]. Primary and secondary windings are uniformly distributed on a former surrounding the sheet and the magnetic field strength is derived from the measured magnetizing current and Ampère's law, assuming a fixed magnetic path length l_m = 0.450 m. Thanks to the large width of the test sample, edge effects are negligible and hardening due to sample cutting can be disregarded. It is a remarkable advantage of SST with respect to the Epstein method, where stress relief annealing of the cut strips is usually required [*35*][*36*]. SST testing of laser-scribed GO Fe-Si can, for example, be directly performed on the treated sheets. Epstein strips should instead be annealed before scribing, in order to keep the beneficial effect of the local deformation by the scratch lines on the domain structure. On the other hand, SST and Epstein methods show comparable reproducibility features, although SST may be more prone to outlying results, ensuing from imperfections, residual magnetism, and loss in the yokes [*37*] [*38*]. Again, the fixed magnetic path length is conducive to a systematic deviation of $P_{SST}(J_p)$ from $P_{eff}(J_p)$, different from and difficult to reconcile with $P_{Epst}(J_p)$ through simple formulation. It is found, in general, that $P_{SST}(J_p) > P_{Epst}(J_p)$, as illustrated for a number of CGO and HGO sheets in Fig. 5.

The typical solution adopted for overcoming the drawbacks associated with the IEC60404-3 standard consists in directly measuring the effective magnetic field strength at the sample surface by means of an *H*-coil. Since this is somewhat impractical with the 500 mm wide sheets, downsized fixtures with strip samples large enough (e.g. 60 mm) to avoid effects from work-hardened edges, have been proposed [*39*][*40*]. *H*-coil measurements are not easy, because a rigid multiturn thin sensor must be realized and accurately calibrated [*41*][*42*] and

the induced signal at power frequencies can be very small and noisy, besides requiring integration. This makes this method appropriate for precise measurements in the laboratory, but unsuitable for the industrial practice. Use of Ampère's law, where the magnetic field strength value is retrieved from the magnetizing current, without incurring in the systematic uncertainty associated with the definition of the magnetic path length in IEC 60404-3 or the difficult handling of *H*-coil low signals, would require some efficient compensation method. By this, we could neutralize the interference of the yokes on the determination of the loss figure, while maintaining zero magnetic potential drop.

B. A novel approach to the compensated SST permeameter.

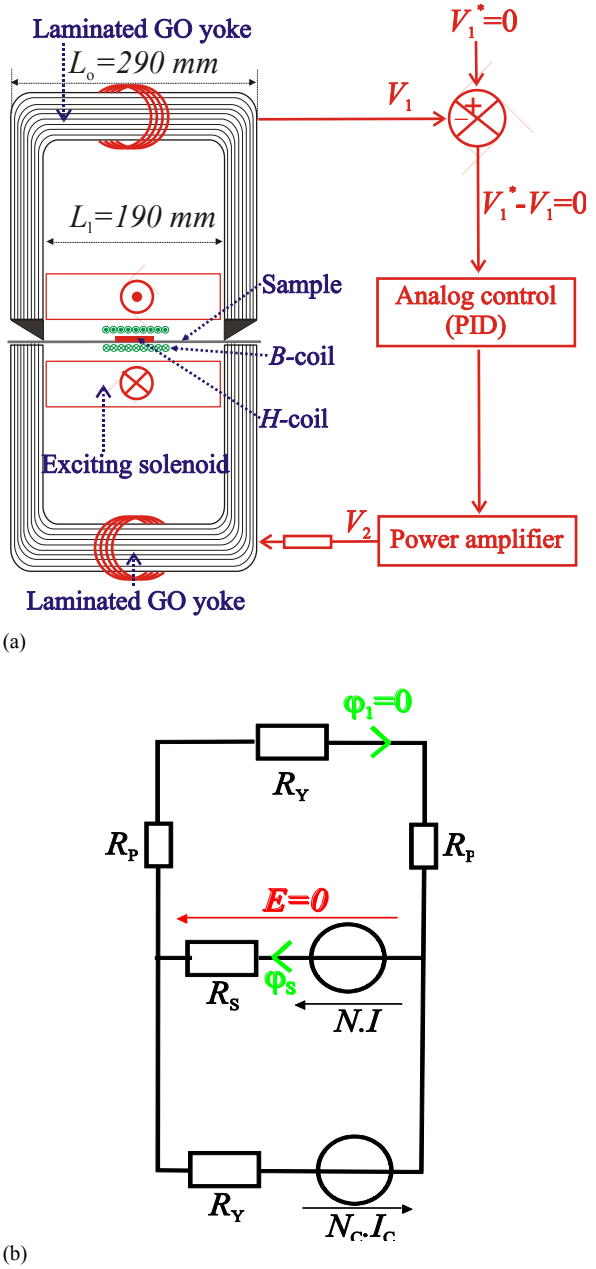

Fig. 6. a) Compensated permeameter with upper yoke working as zero MMF indicator and the related control loop. b) Equivalent reluctance scheme.

The classical compensated DC permeameters, like the Burrows [*43*] and the Iliovici [*44*] permeameters are based on the idea of compensating the drop of magnetomotive force (MMF) occurring in the flux-closing yoke by supplying and suitably adjusting the current flowing in auxiliary windings adjacent to the yoke pole faces. A modern version of AC SST compensated permeameter, discussed in [*45*], is based on the idea of using a Chattock coil, placed upon a defined central portion of length l_m of the sheet sample as a zero signal indicator. The sample is inserted between the pole faces of a double-C laminated yoke and the auxiliary windings are supplied via a high-gain amplifier by the signal generated in the Chattock coil. With magnetizing solenoid and sample suitably longer than l_m, near-zero Chattock signal can be maintained, which implies uniform tangential magnetic field strength over the magnetic path length l_m. A weak point of the Chattock coil method consists in the difficulty of handling the very low signal generated by the coil. We have recently demonstrated that the MMF can actually be controlled with high sensitivity on a defined length of the sample, without using a sensor [*21*]. Such a control is exerted by means of auxiliary windings located on the yoke branches, as sketched in Fig. 6. It works in such a way that the magnetic path length becomes exactly equal to the distance L_1 between the pole faces of the yoke. To this end, the upper yoke is endowed with sharp wedge-shaped pole faces, whose tip lines are in contact with the sample sheet at the precise distance L_1. By imposing that the MMF drop along the upper yoke is zero, one obtains a magnetic path length coincident with L_1, according to the reluctance scheme shown in Fig. 6b. We denote here by R_S, R_Y, and R_P the reluctance of the sample sheet, the lower and upper yokes, and the wedge-shaped poles, respectively. The auxiliary winding on the lower yoke generates the MMF $N_c I_c$, which is controlled in such a way as to cancel the flux circulating in the upper yoke. The PID controller on the feedback loop keeps in fact the voltage $V_1 = d\varphi_1/dt$ detected on the upper yoke vanishingly small by supplying via a high-gain amplifier a magnetizing current to the winding on the lower yoke, where all the flux is eventually deviated. Since the flux in the upper yoke is zero, wedge-shaped bulk poles are perfectly appropriate. The adopted magnetic field strength value $H = Ni/L_1$, for a current i circulating in the exciting N-turn solenoid, is compared with the effective magnetic field strength value, obtained by integrating the voltage simultaneously detected by a many-turn flat *H*-coil placed on the sample surface. By using the yoke itself as a zero MMF indicator, we obtain much larger signal than achievable with the Chattock coil, with ensuing easier and more precise control around the zero value.

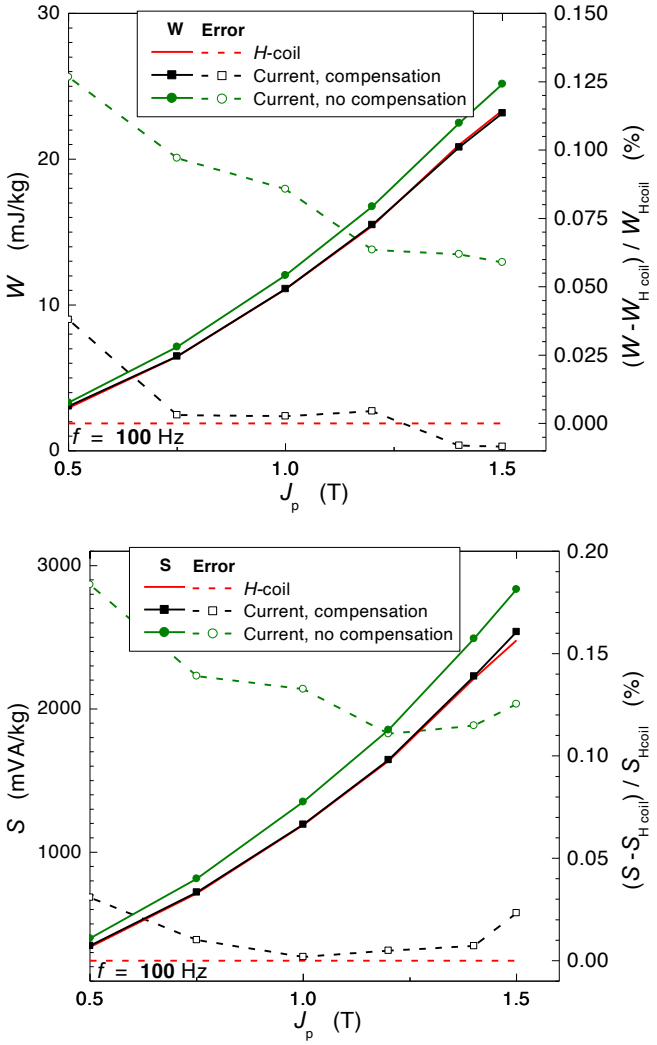

Fig. 7. Energy loss W and apparent power S are measured in GO steel sheets using the newly developed permeameter with and without compensation and with the H-coil method. The measurements are made at 100 Hz as a function of the peak polarization J_p. Compensation leads to drastic reduction of the discrepancies existing between the results obtained with the uncompensated permeameter and the H-coil method.

An example of loss measured at f = 100 Hz by the magnetizing current method, with and without compensation, as a function of peak polarization J_p on GO Fe-Si 30 mm wide strips is given in Fig. 7a. A 50 mm × 50 mm cross-sectional area permeameter is used. The measured loss figures are compared with those obtained by the H-coil method. The discrepancy between the results provided by the compensated permeameter and the H-coil measurements is lower than 1 % beyond J_p = 0.75 T, that is, within the typical measuring uncertainty of the SST method [*8*]. A similar comparison for the apparent power is provided in Fig. 7b.

In summary, the merits of this new type of compensated permeameter can be stated as follows: 1) The loss and apparent power figures are close to the ones measured with the H-coil method; 2) The results are independent of the yoke properties and the reproducibility of the loss figures is in principle ensured, though high permeability GO sheets in the yoke manufacture are recommended for good sensitivity; 3) The effective magnetic field strength is obtained by measurement of the magnetizing current (no need for treating small signals); 4) Only slight modification of standard SST setups is required; 5) This method remains effective at very low frequencies, for which the H-coil method becomes too noisy to get reliable results.

III. Two-Dimensional Magnetization Measurements: Setups and Results

A. Measurement setups

The characterization of soft magnetic sheets under two-dimensional flux has a long story, going back to the end of the 19th century [*46*]. The interest in this type of measurements has chiefly to do with the study of the energy losses in rotating machines [*47*] and three-phase power transformers [*48*][*49*][*50*]. No standards exist for 2D magnetic measurements and a variety of measuring methods are in use [*9*]. This fact, in conjunction with a certain experimental complexity, is the main reason for the substantial discrepancies found in the results from different laboratories [*51*][*52*].

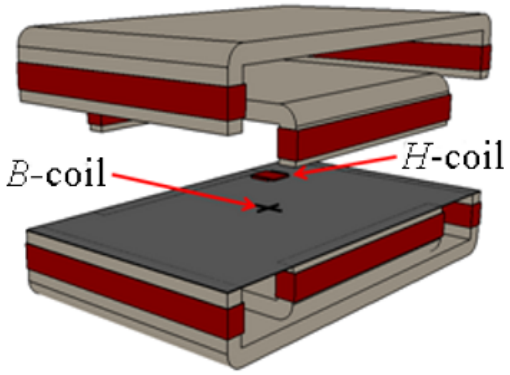

Fig. 8. Example of Vertical Rotational Single Sheet Tester [*53*].

In early attempts to measure the 2D magnetic losses, either cross-shaped samples with orthogonal pickup coils [*54*][*55*] or disk samples placed at the center of two perpendicular rectangular Helmholtz pairs coils supplying a maximum magnetic field strength around 20 kA/m [*56*], were tested. Nowadays, the Rotational Single Sheet Testers (RSST), of either vertical or horizontal type, are typically employed. The vertical RSST derives from the standard SST magnetizer for alternating flux density, to which an orthogonal second double-C yoke is added [*53*][*57*], as sketched in Fig. 8. The magnetizing coils are wound around the yokes and a large sheet sample is generally used, in order to achieve good magnetic field strength homogeneity in the measuring region, typically located at the center of the sample.

The horizontal RSST is realized as a cross-shaped laminated magnetizer with a gap, inside which a square sheet sample is placed [*58*] [*59*] [*60*] [*13*]. It is verified that a square sample ensures better magnetic field strength homogeneity than a circular one [*61*], much more so if the yoke laminations are stacked perpendicular to the sample plane, thereby hindering flux leakage between the adjacent salient poles [*62*][*63*]. Acceptably good flux homogeneity is actually obtained upon a relatively small region across the sample center [*16*] and modifications of the salient poles, supported by Finite Element calculations, have been realized for the sake of widening such a region [*64*] [*15*].

Improved homogeneity of the magnetic flux is obtained by adopting a circular sample inserted in the stator core of a

rotating machine [*52*][*19*][*22*], either two-phase or three-phase. A variant of this approach consists in using an hexagonal sample inside a three-phase magnetizer [*48*][*18*]. The three-phase choice ensures a power advantage in supplying the 2D magnetic field strength (three power amplifiers can be used instead of two) and the flexibility of an additional degree of freedom in the control of the flux loci [*19*]. The price to pay is a certain complexity of the feedback algorithm, requiring a matrix transformation before the conventional fixed point iteration scheme [*65*]. Relatively sophisticated control methods, based on adaptive correction algorithms [*66*], can be found in literature. Other authors prefer simpler methods, even if a non-negligible number of iterations might be required [*67*]. Another interesting variant is the system presented in [*68*]. The rotating flux density is generated by a system of electromagnets working as an array of Halbach magnets. Good homogeneity of the flux density can be reached by such a system.

Recently, 3D magnetizers have been developed, for the specific objective of testing bulk Soft Magnetic Composites (SMC). They are obtained by arranging C-shaped yokes along three orthogonal planes, by which cubic samples can be tested with flux loci lying on a generic plane [*69*].

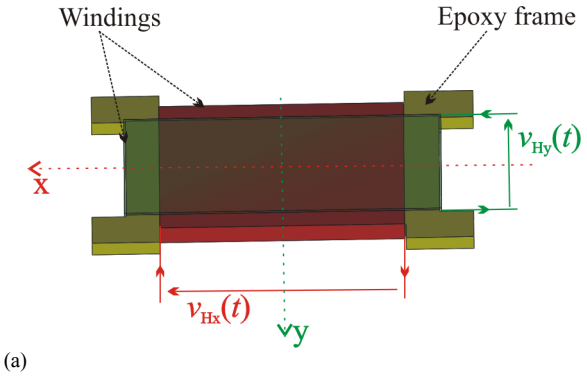

(a)

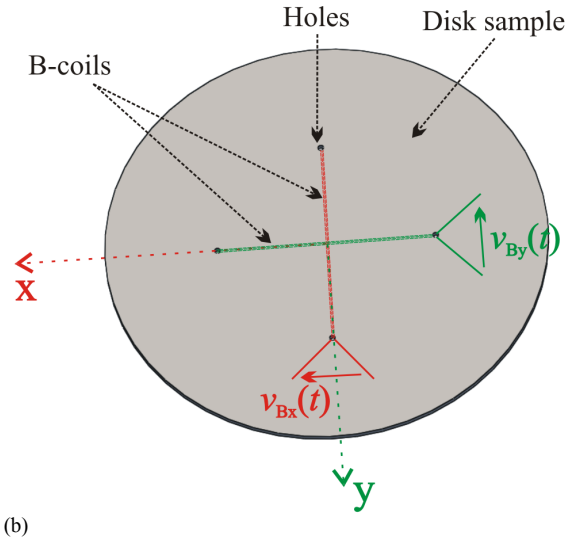

(b)

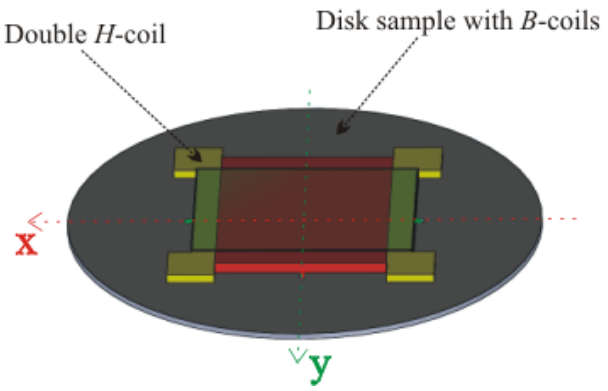

(c)

Fig. 9. Arrangement of *H*- and *B*- windings for the 2D characterization of magnetic sheets. a) Crossed *H*-coils for the measurement of (dH_x/dt, dH_y/dt); b) Crossed *B*-windings, made of few turns threaded through small holes, providing (dB_x/dt, dB_y/dt); c) Final arrangement of the *H*- and *B*- coils for the fieldmetric measurement of 2D hysteresis loops and losses.

B. Measurement of 2D magnetic losses

The measurement of the magnetic losses under a rotating magnetic field strength is typically accomplished on open samples. Consequently, magnetizing current and effective magnetic field strength are in a complex relationship and an *H*-coil is preferably used to determine the magnetic field strength on the measuring area. With the additional knowledge of the local flux density and the usual integration of their product, the loss figure is obtained. This is the rule for 2D loss measurement, but it is in some cases associated with or substituted by the thermometric method [*56*], where the increase of the sample temperature upon energy dissipation is measured.

If we define by x and y the reference axes on the sample plane, the associated (H_x, H_y) magnetic field strength components are thus determined by means of a couple of crossed multiturn flat *H*-coils or by crossed Chattock coils [*70*] [*71*]. The two orthogonal *H*-windings are wound on a rigid thin ($d \sim 1$ mm) epoxy plate, as shown in Fig. 9a. The induced voltages V_{Hx} and V_{Hy} are linked to the magnetic field strength through the equations

$$H_x(t) = \frac{1}{\mu_0 (NA)_x} \cdot \int V_{Hx}(t)\, dt$$
$$H_y(t) = \frac{1}{\mu_0 (NA)_y} \cdot \int V_{Hx}(t)\, dt \qquad (6)$$

where $(NA)_x$ and $(NA)_y$ are the turn-area products of the coils. With uniform flux density in the measuring area, tangential ($H_x(t)$, $H_y(t)$) and effective magnetic field strength components coincide and associate with the components (B_x, B_y). These are typically obtained by threading a couple of few-turn windings through small (0.5-0.75 mm) holes drilled symmetrically on the measuring region, as illustrated for a disk sample in Fig. 9b. The flux density components are then calculated from the detected e.m.f.s ($V_{Bx}(t)$,$V_{By}(t)$), according to

$$B_x(t) = \frac{1}{N_{Bx}A_x}\cdot\int V_{Bx}(t)\,dt$$
$$B_y(t) = \frac{1}{N_{By}A_y}\cdot\int V_{By}(t)\,dt \qquad (7)$$

where N_{Bx} and N_{By} are the number of turns of the *B*-windings, and (A_x, A_y) are the linked cross-sectional areas of the material. To avoid drilling the sample and the possible perturbations induced by this process (which can in any case be removed by annealing), the needle method, where point-like contacts are made in place of holes and the related voltage drop is detected, has been implemented [*72*][*73*]. The detected signal, however, is generally very low and noisy, and this method is not in general use.

The precise measurement of ($B_x(t)$,$B_y(t)$) requires the accurate determination of the cross-sectional areas (A_x, A_y) linked with the *B*-windings. Given the rounded profile of the holes, the geometrical determination of (A_x, A_y) in the sheet samples can be inaccurate. In addition, on approaching very high polarization values, precise correction for the air-flux is required, but the actual turn-area of the *B*-coils is not accurately known. For its precise determination, the saturation polarization of the material is first measured by a standard method (e.g., using a permeameter) on a conventional strip sample with well-known cross-sectional area. The disk sample is then inserted between the pole faces of a Type-B permeameter ([*9*], pp. 311) and the flux $\Phi_x = N_{Bx}(JA_x+\mu_0 HA_t)$, where J is the polarization and A_t is the total area (air plus sample) linked with the B_x winding, is measured. The effective magnetic field strength H, measured at the coil position by means of a Hall plate, is increased beyond about 150 kA/m, thereby ensuring full magnetic saturation $J = J_S$. The linear increase of Φ_x versus H is exclusively due to the term $\mu_0 HA_t$ in high-magnetic field strength region. We obtain in this way the area A_t and, for any sufficiently high magnetic field strength H_0, the measuring cross-sectional area of the sheet sample

$$A_x = \frac{\Phi_x(H_0) - N_{Bx}\mu_0 H_0 A_t}{N_{Bx}J_S} \qquad (8)$$

By repeating the same procedure along the *y*-direction, A_y is obtained and the loss can finally be calculated from the measured magnetic field strength and flux density components and their time dependence according to the Poynting theorem

$$W = \int_0^T \left(H_x\frac{dB_x}{dt} + H_y\frac{dB_y}{dt}\right)dt \qquad [\mathrm{J/m^3}] \qquad (9)$$

To remark here the inevitable approximation involved with the measurement of the effective magnetic field strength in the open sample, with its large and relatively inhomogeneous demagnetizing field. The *H*-coil provides, because of its finite thickness, an overestimate of the true magnetic field strength value in the sample. This fact, however, does not interfere with the loss measurement, because true and measured magnetic field strengths differ by a quantity proportional to the magnetization.

A further drawback of the fieldmetric 2D loss measurement can derive from possible slight misalignment and imperfect orthogonality of the *H*- and *B*- windings [*74*] [*75*] [*76*]. This leads to different loss values when measured with the magnetic field strength rotating clockwise (CW) or counterclockwise (CCW). While the difference is reduced, though not negligibly [*77*], at low flux density values, dramatic divergence between CW and CCW rotational losses can be observed at high flux densities (e.g., beyond 1.5 T in non-oriented alloys) [*77*] [*78*]. This discrepancy can be largely, though not fully, compensated by averaging the results of the CW and CCW measurements [*79*][*80*][*78*], as the geometrical phase lag is reversed relatively to the electromagnetic phase lag.

At high flux densities, the phase shift between flux density and magnetic field strength (actually, its fundamental harmonic) may become too small to be measured with sufficient accuracy. Consequently, the thermometric method, where the magnetic power loss is associated with the rate of heating of the sample, would rather be used rather than the usual fieldmetric method. In the ideal case of adiabatic measurements on a material of specific heat c_p, the power loss per unit mass is related to the time derivative of the temperature according to

$$P = c_p \cdot dT/dt \qquad [\mathrm{W/kg}] \qquad (10)$$

The temperature is measured either with a thermocouple stuck on the sheet surface [*9*][*56*] or a thermistor [*81*]. Good agreement between the fieldmetric method and the thermocouple-based thermometric method is verified in NO steel sheets [*20*]. The thermistor sensors actually appear better suited to localized loss investigations, as those concerning high-permeability wide-domains GO steels [*81*].

C. 2D magnetizers for high frequencies and high flux densities: design and analysis

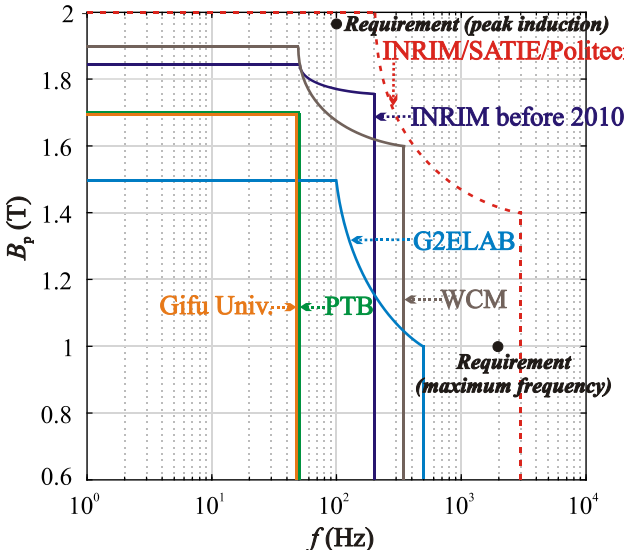

Fig. 10. Basic 2D measuring capabilities on non-oriented steel sheets by international laboratories are summarized in the B_p vs. frequency plane. The dashed line defines the enhanced upper limit jointly achieved by INRIM/SATIE/Politecnico di Torino.

The relative complexity of the 2D measurements, due to the open sample configuration, the related need for bulky magnetizers, and the relatively awkward control of the flux loci, have traditionally limitated the range of frequency and flux density B_p. This becomes apparent when the reported capabilities of the main laboratories dealing with the 2D characterization of nonoriented steel sheets are considered and

compared, as shown in the peak flux density versus test frequency map shown in Fig. 10. The maximum experimental frequency is typically around a few hundred Hz and reliable results are hardly obtained beyond 1.7 T – 1.8 T [*78*]. The reported 2D measuring limits regard INRIM (before year 2010) [*19*][*20*], Wolfson Centre WCM [*82*], G2ELAB Grenoble [*83*][*84*], PTB Braunschweig [*85*], Gifu Univ. [*86*]. Actually, present-day high-speed rotating machines involve frequencies in the kHz range [*87*]), and mass reduction requirements force machine designers to deal with flux density levels around 2 T, as highlighted in Fig. 10. The dashed line in this figure, covering such (B_p, f) limiting profile, reflects the enhanced 2D measuring capabilities recently attained by the joint efforts of the SATIE/INRIM/Politecnico di Torino labs. Two magnetizers have been designed, built, and employed for this purpose. We summarize in the following the properties of these devices, the related measuring methods, and a few significant results.

1) The high-frequency 2D magnetizer

A two-pole three-phase machine has been designed for 2D magnetic testing up to the kilohertz range of disk-shaped samples. A 3D FEM calculation has been conducted and optimized machine geometry has been designed for an 80 mm diameter sample. The calculations take into account the specifications of the supply system, consisting of three CROWN AUDIO 5000VZ power amplifiers (peak-to-peak output voltage 300 V, maximum output current 40 A), driven by three synchronized Agilent 33220a function generators. The feedback system employed for the control of flux density loci is based on the contraction mapping principle [*65*]. The scheme of the magnetizer and the adopted 3D FEM meshing is shown in Fig. 11, together with the actual device. This is equipped with a toroidal winding, which avoids long overhangs. Three slots per pole are used, totaling 18 slots. The laminated core is made of 0.35 mm thick non-oriented Fe-Si sheets, whose experimental anhysteretic curve is taken as magnetic constitutive equation of the material in the FEM calculations. Details on the modeling criteria and procedure are discussed in [*88*]. Two main points are stressed here:

1. The disk sample is separated from the magnetizing core by a 1 mm thick gap. This narrow air gap allows to minimize the apparent power required by the magnetizer.
2. The axial height T of the magnetizing core is optimized by 3D FEM calculations to maximize the flux density in the sample under a given magnetizing power. By taking the anhysteretic constitutive equation for a standard type of non-oriented sample of thickness d, the calculations show, in particular, that, for a ratio $T/d \sim 75$, minimum apparent power is required in order to achieve a defined peak flux density value (e.g. $B_p = 1.5$ T at 1 kHz). For $d = 0.20$ mm, a 15 mm thick core is therefore predicted.

For measurements performed with the fieldmetric method, a 1 mm thick 20 mm × 20 mm crossed H-coil, placed in the central region of the disk sample, is employed. The capacitive effects are minimized by adequately spacing the turns, for kHz range operation.

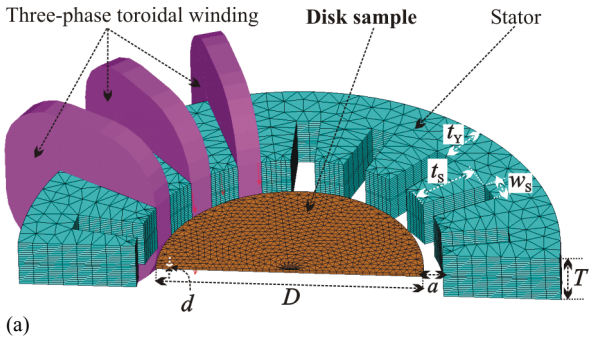

(a)

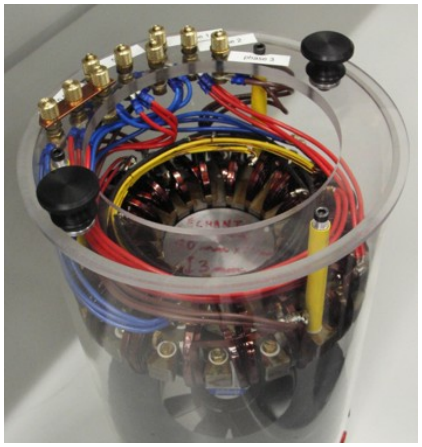

(b)

Fig. 11. Three phase magnetizer designed for 2D magnetic measurements up to the kHz range. a) Schematic view and 3D FEM model. b) Assembled setup with test sample (adapted from [*88*]).

The need for open samples and the relatively small T/d ratio might have detrimental effects on the uniformity of the flux density across the measuring region. This should then be preemptively verified, as done in the present case by 3D FEM analysis. An example is here provided, where, according to Fig. 12, we take the reference axes (x, y) originating at the center of the disk sample and we regulate phase and amplitude of the magnetizing currents in such a way that unidirectional magnetization along the y-axis is obtained, averaging to B_p = 1.5 T along the 40 mm wide measuring region covered by the $B_y = B_y(x, y = 0)$ coil. The calculated flux density $B_y(x,y = 0)$, which behavior through the whole disk width is plotted in Fig. 13, turns out to be quite uniform across such a region (0.2% of relative difference).

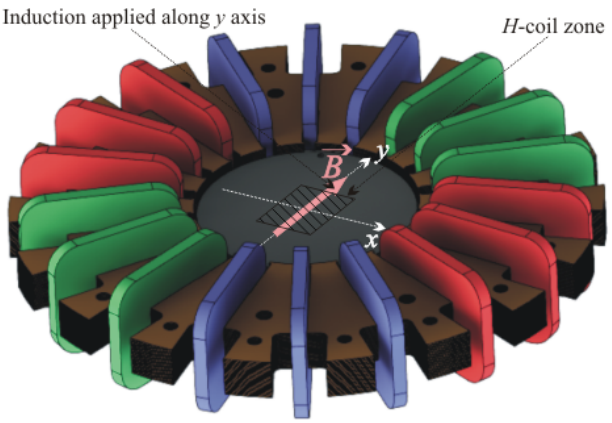

Fig. 12. An axis system *x*-*y* is defined on the sample surface. The three-phase currents are set in such a way that an alternating flux density of peak value B_p = 1.5 T is established along the *y* axis. The shadowed 20 mm square region centered on the sample surface is the *H*-coil zone.

The same 3D FEM analysis was used to evaluate the uniformity of the effective magnetic field strength at the sample surface. Fig. 14 provides the behavior of $H_y(x,y)$, paralleling the dependence of $B_y(x, y = 0)$ shown in Fig. 13, on the square centered region of size 40 mm (a) and the inner square region of size 20 mm (b). The inhomogeneity of the magnetic field strength (about 31% decrease from $y = 0$ to $y = \pm 20$ mm) with respect to the flux density is inevitably due to the strong non-linearity of the $B(H)$ dependence at J_p = 1.5 T. In order to have good congruence between the *B* and *H* signals, a square 20 mm sized *H*-coil is adopted. This analysis leads to similar results and conclusions for the high-flux density 2D magnetizer, to be discussed in the following.

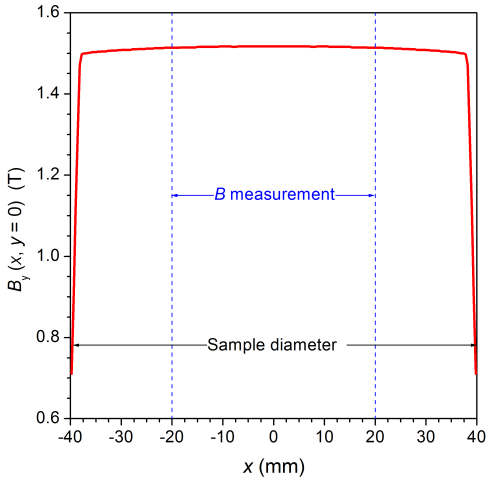

Fig. 13. Behavior of the magnetic flux density $B_y(x, y = 0)$ across the 80 mm *x*-diameter of the non-oriented Fe-Si disk sample calculated for alternating magnetic field strength directed along the *y*-diameter. The *B*-measuring region is restricted to the -20 mm ≤ x ≤ 20 mm region. The relative difference between $B_y(0,0)$ and $B_y(\pm 20$ mm,0) is equal to 0.2%.

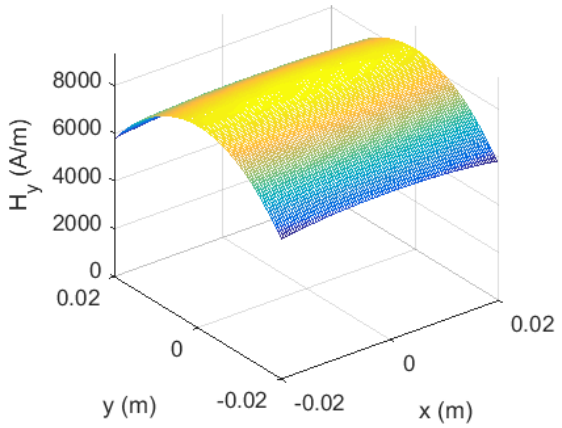

(a)

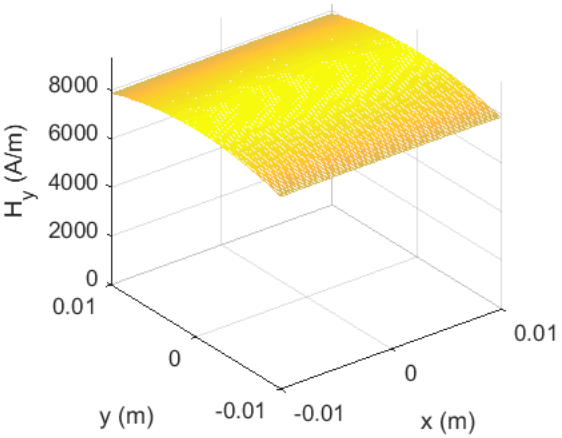

(b)

Fig. 14: Condition B_x=0, B_y=1.5 T, as in Fig. 12. a) Magnetic field strength homogeneity $H_y(x,y)$ calculated by FEM analysis on the sample surface over a 40 mm wide centered square region. b) Enlarged view of the inner 20 mm wide area. The relative 31 % difference found between $H_y(0, x)$ and $H_y(\pm 20$ mm, $x)$ is reduced to 7 % for $H_y(\pm 10$ mm, $x)$.

2) The high-flux density 2D magnetizer

In order to fully cover the aimed at (*B*, *f*) domain envisaged in Fig. 10, a novel magnetizer, specifically designed for 2D measurements at high flux densities, was developed. In such a device, the basic structure of the previous high-frequency magnetizer was retained, together with the 80 mm diameter sample. However, with the same two-pole/three-phase 18 slot configuration, re-sizing of the magnetizer was required. The thermometric measurements at high flux densities, in fact, are preferably performed under near-adiabatic conditions, which are in the present case emulated by keeping the sample inside a vacuum bell ($p \sim 10^{-3}$ Pa), which occupies the stator bore, as sketched in Fig. 15. The 6 mm thick walls of the vacuum chamber, made of PVC, introduce a relevant airgap and the optimized *T/d* ratio will differ from the value found for the previous setup. An additional constraint is posed by the maximum current of 40 A per phase delivered by the CROWN AUDIO 5000VZ power amplifiers (little constraint on the voltage is posed at power frequencies). By keeping the previous winding scheme, the magnetomotive force (MMF.) per slot necessary to reach B_p = 2 T at the sample center has been computed by FEM analysis as a function of *T/d* [*88*]. From the results shown in Fig. 16, obtained with *d* = 0.20 mm, the optimized value *T/d* = 150, that is *T* = 30 mm, is estimated, with

the MMF. per slot around 1000 A. This condition is satisfied, taking into account the 40 A upper limit for the magnetizing current, by inserting 25 turns per slot. Assuming a maximum current density of 5 A/mm^2 (forced air convection is used to cool the windings), the geometrical parameters of teeth and back core of the magnetizer are then calculated, as summarized in Table I. To remark that the thermal transfer due to Joule heating of the windings and their forced cooling does not influence the temperature of the sample, which is protected in the vacuum chamber.

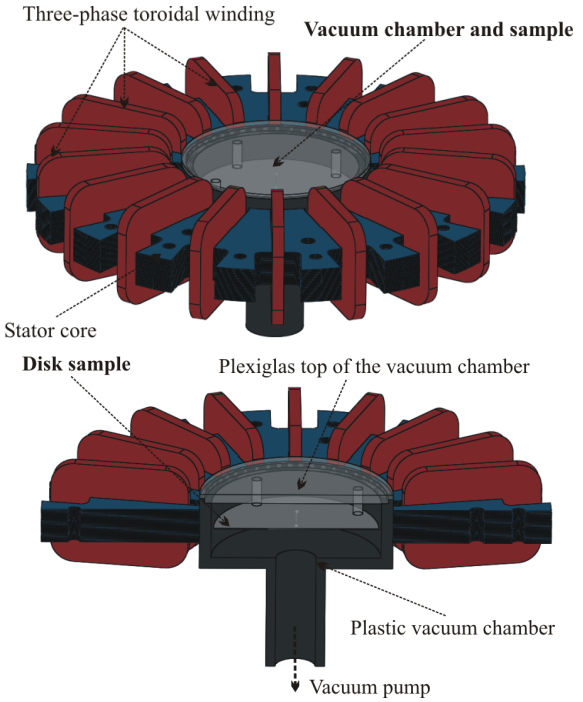

Fig. 15. Front and cross-sectional views of the high-flux density magnetizer. It holds the vacuum chamber employed for emulating quasi-adiabatic conditions during the measurement of the magnetic power loss with the thermometric method.

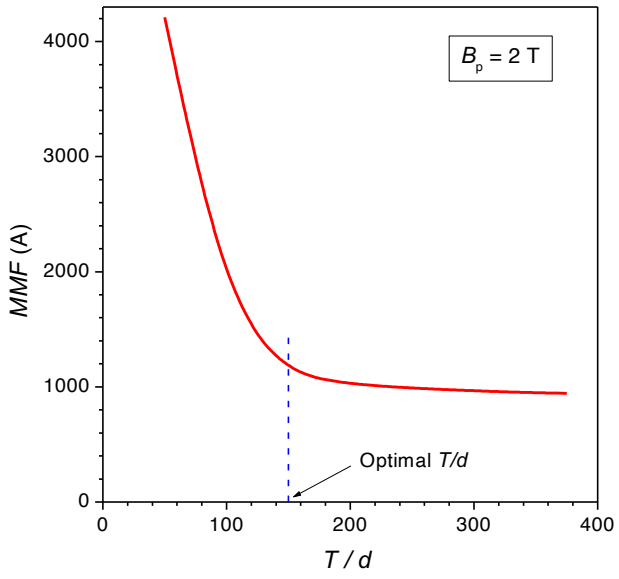

Fig. 16. Magnetomotive force per slot required to reach $B_p = 2$ T at the center of the 0.20 mm thick disk sample as a function of the ratio T/d between axial height of the magnetizer and sample thickness.

TABLE I

GEOMETRICAL PARAMETERS OF THE MAGNETIZER DESIGNED FOR MEASUREMENTS AT HIGH FLUX DENSITIES

Parameter	Symbol	Value
Sample diameter	D	80 mm
Airgap thickness	a	6 mm
Magnetizer axial thickness	T	30 mm
Teeth depth	t_S	45 mm
Teeth width	w_S	15 mm
Yoke thickness	t_Y	20 mm
Number of turns per coil	N	25

As previously, stressed, the large uncertainty of the loss value measured by the conventional fieldmetric method at high flux densities can be overcome by measuring the dissipated power through the rise of the sample temperature. This can be easily detected, in particular, by a copper-constantan extended junction, carefully glued by silver paint on the sample surface, along and close to the *B*-windings. The reading of the junction signal is made by a calibrated nanovoltmeter, which output signal upon switch-on and switch-off of the magnetic field strength displays the typical behavior shown in Fig. 17. The magnetic field strength is applied at time t_{on}, after stabilizing the whole device temperature, and switched off at time t_{off}. The temperature difference between the temperature at a certain instant t and the one at time t_{on} is called □□. Since the system is not fully adiabatic, we observe a typical first order system increase of □□ vs. t till switch-off at time $t = t_{off}$, followed by an exponential decrease. Consequently, (10) does not apply, but we can nevertheless precisely retrieve the power loss figure by modeling the heat exchange process according to the balance equation

$$P = \frac{dQ_{in}}{dt} + \frac{dQ_{out}}{dt} = c_p \frac{d\Delta\theta}{dt} + K_{ext}\Delta\theta, \ (t > t_{on}) \qquad (11)$$

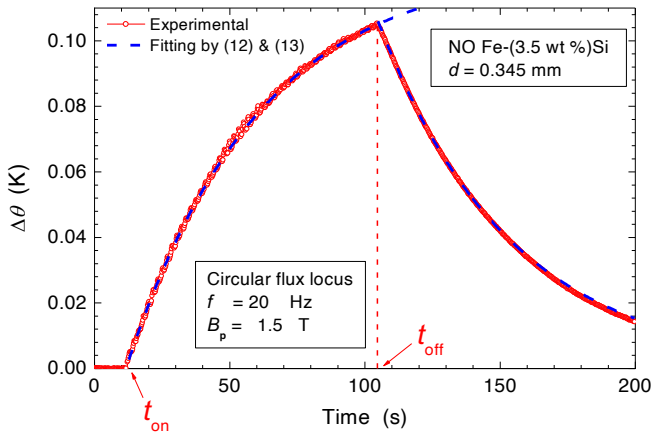

Fig. 17.: Temperature versus time in a non-oriented Fe-Si alloy subjected to rotational magnetic field strength at 20 Hz from time t_{on} to time t_{off}. The temperature difference □□*(t)* follows an exponential dependence on time, with time constant $\tau = c_p/K_{ext}$, where c_p is the specific heat of the alloy and K_{ext} is the heat transmission coefficient, by which we lump the imperfect adiabatic response of the sample. The continuous fitting lines are calculated from (12) and (13).

where we denote by dQ_{in}/dt and dQ_{out}/dt the rates at which heat is stored in the sample and lost to the environment, respectively, and by K_{ext} the heat transmission coefficient. The increase of the specimen temperature T with time is then obtained from (11) as

$$\Delta\theta = \frac{P}{K_1}\cdot\left[1-\exp\left(-\frac{K_{ext}}{c_p}(t-t_{on})\right)\right],(t_{on} \le t \le t_{off}) \qquad (12)$$

In the limit $K_{ext} \to 0$, this equation reduces to the linear relationship (10). The coefficient K_{ext} is unknown, but it can be found by fitting the exponential decay of temperature observed after switch-off. If at the instant of time t_{off} the temperature difference is $\Delta\theta_1$, the time dependence of the temperature difference is obtained, by posing $P = 0$ in (11), as

$$\Delta\theta = \Delta\theta_1\cdot\exp\left(-\frac{K_{ext}}{c_p}(t-t_{off})\right),(t > t_{off}) \qquad (13)$$

We find that the temperature decay is accurately described by (13), with the time constant $\tau = c_p/K_{ext}$. For the specific case of the Fe-(3.5wt%)Si sheet sample of Fig. 17, having specific heat c_p = 470 J·kg^{-1}·K^{-1}, we obtain from (13) the time constant τ = 48.7 s and K_{ext} = 9.65 J·kg^{-1}·K^{-1}·s^{-1} The value of P is then determined by fitting through (12) the experimental $\Delta\theta$ vs. t increase in the time interval (t_{off} – t_{on}). It is noted that, by limiting the measurement to very short times (t_{off} – t_{on}) << τ (τ = 49 s in Fig. 17) a straight line is a good approximation to (12) and we can retrieve P by (10). In the example reported in Fig. 17, we find by (12) P = 1.16 W/kg.

3) A few significant results

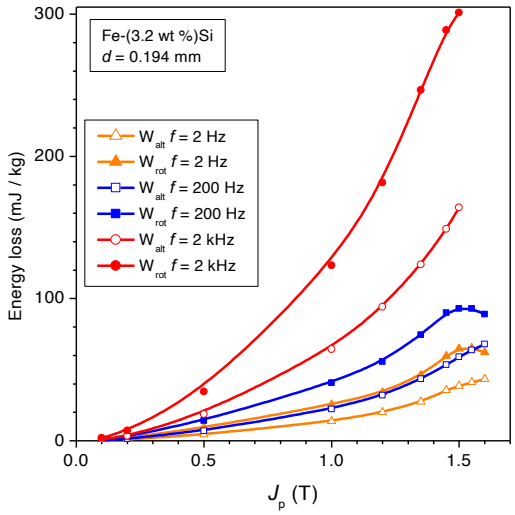

(a)

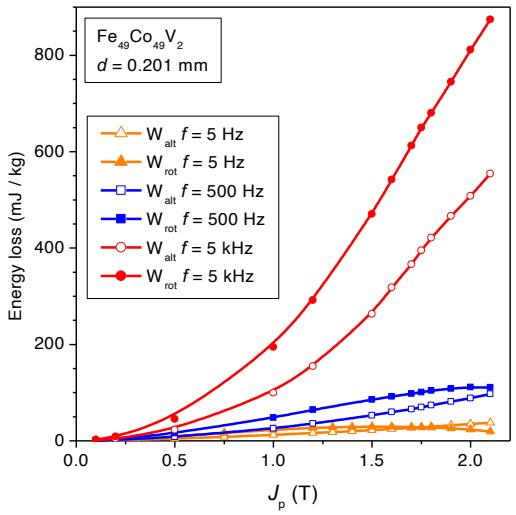

(b)

Fig. 18. Alternating W_{alt} and rotational W_{rot} energy losses measured with the use of the high-frequency RSST magnetizer in Fe-Si (a) and Fe-Co (b) non-oriented steels sheets up to the kHz range.

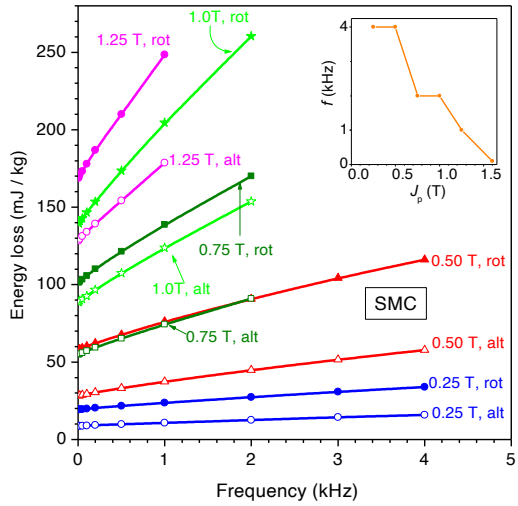

Fig. 19. Broadband energy loss under alternating and circular magnetic polarization measured with the high-frequency RSST in a Soft Magnetic Composite. The curve shown in the inset roughly delimits the accessible (f, J_p) measuring domain.

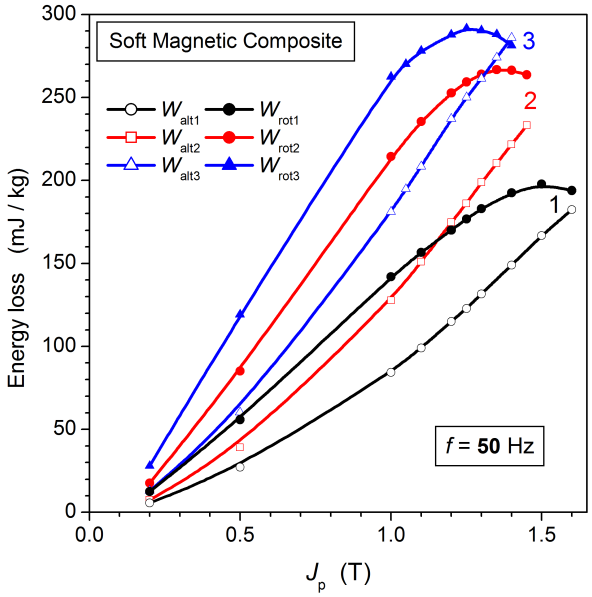

Fig. 20. Alternating W_{alt} and rotational W_{rot} energy loss measured at 50 Hz in three different types of Fe-based Soft Magnetic Composites. They are subjected to different preparation treatments, leading to different mass densities δ. They attain the values: δ_1 = 7450 kg/m^3, δ_2 = 7260 kg/m^3, δ_3 = 7110 kg/m^3.

The high-frequency RSST magnetizer has been used for unidirectional and 2D loss measurements up to the kHz range in steel sheets and Soft Magnetic Composites (SMC). Fig. 18 provides an example of measured alternating W_{alt} and rotational (circular flux loci) W_{rot} losses in 0.20 mm thick non-oriented Fe-Si (up to 1.5 T / 2 kHz) and Fe-Co (up to 2.1 T / 5 kHz) sheets. The skin effect under alternating and circular polarization is put in evidence at the highest frequencies [*89*] [*90*]. One can notice in Fig. 18 the progressive disappearance of the maximum of W_{rot} vs. J_p on increasing the magnetizing frequency. This behavior is understood in terms of growing share of the classical loss component in the total loss, a quantity monotonically increasing with J_p [*23*]. Measurements of W_{alt} and W_{rot} at high frequencies in SMC materials, which, because of their granular structure, are expected to bear some advantage in terms of loss behavior, are reported in Fig. 19. The 80 mm diameter tested SMC disks have a thickness of 3 mm. Because of their low permeability (μ_r ~ 100 - 500) and bulk shape, these materials pose a challenge to their 2D characterization at medium-to-high flux densities and frequency values in the kHz range. The domain (f, J_p) accessible to measurements can be roughly identified with the area subtended by the experimental limiting $f(J_p)$ line shown in the inset of Fig. 19. This measuring capability is superior to the state of the art [*91*]. Typical behaviors at 50 Hz (i.e., close to quasi-static excitation) of W_{alt} and W_{rot} versus J_p in different types of SMC are shown in Fig 20. These samples have been obtained following different processes, leading to different average particle size and density δ. It is observed how the loss increases with decreasing material density (from δ = 7450 kg/m^3 to δ = 7110 kg/m^3 on passing from sample 1 to sample 3), that is, increasing the thickness of the intergrain boundaries. At the same time, W_{rot} moves its maximum value to lower J_p values. Grain decoupling, ensuing from thicker non-magnetic boundaries, yields higher coercivity (i.e. higher quasi-static losses). On the other hand , the coherent moment rotations also start at lower J_p values, because the required applied magnetic field strength, largely increased to compensate higher internal demagnetizing fields, becomes high enough to induce coherent rotations in the favored grains

The high-flux density magnetizer shown in Fig. 15 permits to approach the magnetic saturation under alternating and two-dimensional magnetic field strengths in steel sheets. To this end, both fieldmetric and thermometric methods are applied upon the low- and high-flux density range, respectively. An example is provided in Fig. 21, concerning the behavior of W_{alt} and W_{rot} in a non-oriented Fe-(3 wt %)Si sample, brought up to B_p = 2.0 T (J_p = 1.95 T). The fieldmetric method is applied up to about 1.6 T, the thermometric method beyond this limit, with a short overlap region. The capability of this system to measure the value of W_{rot} very close to the saturated state allows reaching the limiting condition, where domain walls collapse, and only coherent reversible rotations are deemed to provide the macroscopic rotation of the magnetization. In this case, the measured loss should reduce to the classical loss component, according to the equation

$$W_{rot} = W_{rot,class} = \frac{\pi^2}{3} \cdot \frac{\sigma d^2 B_p^2}{\delta} f \qquad [J/kg] \qquad (14)$$

where σ is the electrical conductivity, and d and δ are the previously introduced sheet thickness and density, respectively. Using (14) and the experimental $W_{rot}(f)$ behavior at different J_p values [*23*], we can separate $W_{rot}(J_p)$ in the NO Fe-Si sheet of Fig. 21 into its hysteresis $W_{hyst}(J_p)$, excess $W_{exc}(J_p)$, and classical $W_{class}(J_p)$ components up to saturation, as shown in Fig. 22. Here we prove that by (14) we identify the limiting value of the rotational loss for $J_p = J_s$, a previously predicted result.

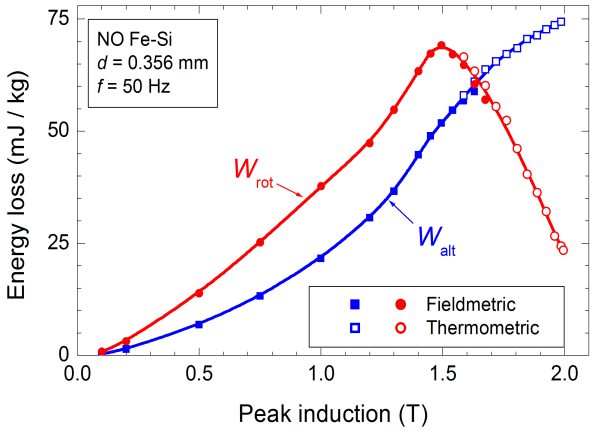

Fig. 21. Alternating W_{alt} and rotational W_{rot} energy losses in NO Fe-Si sheets measured at 50 Hz up to peak flux density B_p = 2.0 T (J_p = 1.95 T).

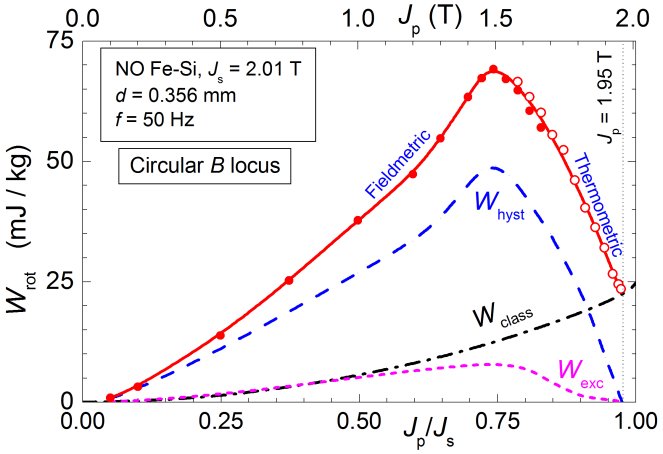

Fig. 22. Loss separation under rotating flux density up to $J_p = 0.97Js$ in a 0.356 thick NO Fe-Si sheet.

IV. Conclusions

We have discussed the problems connected with the measurement of the magnetic properties of soft magnetic materials under alternating and two-dimensional magnetic field strengths and related recent advances, with a focus on recent investigations and advances obtained by the cooperative activity of the SATIE, INRIM, and Politecnico di Torino labs.

The Epstein and SST standard measuring methods and the systematic deviations of their power loss figures from the true values, follow from the specifically involved magnetic circuits and the practical need to define a magnetic path length. This, however, inevitably depends on the sample type, the flux density level, and the magnetizing frequency. Detailed analysis of the Epstein measurements made on different NO and GO Fe-Si sheets shows, for example, that in all materials the effective magnetic path length increases with the peak polarization, differing by up to about 5 % with respect to the standard 0.94 m path length [*10*]. A Single Sheet Tester with double-C flux-closing yoke has therefore been developed, by which the magnetic path length is independent of the material type and flux density level by means of an original compensation method, based on the use of the yoke itself as a zero-MMF indicator. Systematic deviations from the true loss values are in this way reduced to less than 1 %, that is within the typical uncertainty of this kind of measurements.

The present-day capabilities of the two-dimensional measuring systems lack in general the access to frequencies in the kHz range at technical flux densities and to high flux densities at power frequencies. But testing at high frequencies and high flux densities meets the demand by today machine designers. To overcome current limitations, the authors have developed novel setups, based on 3D FEM designed three-phase magnetizers, employed with disk-shaped samples, minimum airgap, high-performance power amplifiers, and dedicated feedback algorithms. Loss measurements up to 2 kHz at 1.5 T could be made, for example, in 0.20 mm thick non-oriented Fe-Si sheets, a range broadened to 2.1 T and 5 kHz in the high-saturation Fe-Co alloys. Soft Magnetic Composites could also be tested up to 1 kHz at 1.25 T. These figures largely exceed previous literature reports. On the other hand, the saturation magnetization could be closely approached in non-oriented Fe-Si sheets at power frequencies. It is here verified, in particular, that W_{rot} is reduced to the classical component, as expected on theoretical grounds, but never experimentally proved.

V. References

[1] P. Di Barba, M. Bonislawski, R. Palka, P. Paplicki, and M. Wardach, "Design of hybrid excited synchronous machine for electrical vehicles," *IEEE Transactions on Magnetics*, vol. 51, no. 6, pp. 1-6, 2015.

[2] W. Hua, G. Zhang, and M. Cheng, "Investigation and design of a high-power flux-switching permanent magnet machine for hybrid electric vehicles," *IEEE Transactions on Magnetics*, vol. 51, no. 3, pp. 1-5, 2015.

[3] D. Kowal, P. Sergeant, L. Dupré, and L. Vandenbossche, "Comparison of iron loss models for electrical machines with different frequency domain and time domain methods for excess loss prediction," *IEEE Transactions on Magnetics*, vol. 51, no. 1, pp. 1-10, 2015.

[4] IEC Standard Publication 60404-2 Edition 3, Part 2: Methods of measurement of the magnetic properties of electrical steel strip and sheet by means of an Epstein frame, 2008-06, Geneva, IEC Central Office (ISBN 2-8318-9835-8).

[5] IEC Standard Publication 60404-10 Edition 2.0, Part 10: Methods of measurement of magnetic properties of magnetic steel sheet and strip at medium frequencies, 2016-10, Geneva, IEC Central Office (ISBN 978-2-8322-3725-0).

[6] IEC Standard Publication 60404-3 Edition 2.2, Part 3: Methods of measurement of the magnetic properties of electrical steel strip and sheet by means of a single sheet tester, 2010-04, Geneva, IEC Central Office (ISBN 978-2-88910-186-3).

[7] J. Sievert et al., "Magnetic measurements on electrical steels using Epstein and SST methods," *PTB-Bericht*, vol. E-74, pp. 1-28, 2001.

[8] C. Appino et al., "International comparison on SST and Epstein measurements in grain-oriented Fe-Si sheet steel," *International Journal of Applied Electromagnetics and Mechanics*, vol. 48, no. 2-3, pp. 123-133, 2015.

[9] F. Fiorillo, *Measurement and characterization of magnetic materials*.: North-Holland, 2004.

[10] E. Ferrara et al., "Effective versus standard Epstein loss figure in Fe-Si sheets," *International Journal of Applied Electromagnetics and Mechanics*, vol. 55, no. S1, pp. 105-112, 2017.

[11] T. Sasaki, M. Imamura, S. Takada, and Y. Suzuki, "Measurement of rotational power losses in silicon-iron sheets using wattmeter method," *IEEE Transactions on Magnetics*, vol. 21, no. 5, pp. 1918-1920, 1985.

[12] A. Abou-Elyazied Abdallh, P. Sergeant, and L. Dupré, "A Non-Destructive Methodology for Estimating the Magnetic Material Properties of an Asynchronous Motor," *IEEE Transactions on Magnetics*, vol. 48, no. 4, pp. 1621-1624, 2012.

[13] M. Enokizono, T. Suzuki, J. Sievert, and J. Xu, "Rotational power loss of silicon steel sheet," *IEEE Transactions on Magnetics*, vol. 26, no. 5, pp. 2562-2564, 1990.

[14] J.G. Zhu and V.S. Ramsden, "Two dimensional measurement of magnetic field and core loss using a square specimen tester," *IEEE Transactions on Magnetics*, vol. 29, no. 6, pp. 2995-2997, 1993.

[15] D. Makaveev, M. von Rauch, M. De Wulf, and J. Melkebeek, "Accurate field strength measurement in rotational single sheet testers," *Journal of Magnetism and Magnetic Materials*, vol. 215-216, pp. 673-676, 2000.

[16] N. Nencib, A. Kedous-Lebouc, and B. Cornut, "2D analysis of rotational loss tester," *IEEE Transactions on Magnetics*, vol. 31, no. 6, pp. 3388-3390, 1995.

[17] M. Enokizono, T. Todaka, T. Sashikata, J. D. Sievert, and H. Ahlers, "Magnetic field analysis of rotational loss tester with vertical yoke," *Journal of Magnetism and Magnetic Materials*, vol. 112, no. 1-3, pp. 81-84, 1992.

[18] A. Hasenzagl, B. Weiser, and H. Pfützner, "Novel 3-phase excited single sheet tester for rotational magnetization," *Journal of magnetism and magnetic materials*, vol. 160, pp. 180-182, 1996.

[19] C. Appino, F. Fiorillo, and C. Ragusa, "Loss decomposition under two-dimensional flux loci in non-oriented steel sheets," *Przegläd Elektrotechniczny*, vol. 83, pp. 25-30, 2007.

[20] C. Appino, F. Fiorillo, and C. Ragusa, "One-dimensional/two-dimensional loss measurements up to high inductions," *Journal of Applied Physics*, vol. 105, no. 7, p. 07E718, 2009.

[21] O. de la Barriere et al., "A simple compensation method for the accurate measurement of magnetic losses with a single strip tester," *IEEE Transactions on Magnetics*, vol. 52, no. 16, pp. 1-4, 2016.

[22] V. Gorican, "2-D measurements of magnetic properties using a round RSST," in *Proceedings of the 2000 International Workshop on 1&2-Dimensional Magnetic Measurement and Testing*, Bad Gastein, 2000.

[23] C. Appino, M. Khan, O. de la Barrière, C. Ragusa, and F. Fiorillo, "Alternating and Rotational Losses up to Magnetic Saturation in Non-Oriented Steel Sheets," *IEEE Transactions on Magnetics*, vol. 52, no. 5, pp. 1-4, 2016.

[24] O. de la Barrière et al., "Loss separation in soft magnetic composites," *Journal of Applied Physics*, vol. 109, no. 7, p. 07A317, 2011.

[25] IEC Standard Publication 60404-4 Edition 2.2, Part 4: Methods of measurement of d.c. magnetic properties of iron and steel, 2008-11, Geneva, IEC Central Office (ISBN 978-2-88910-188-7).

[26] IEC Standard Publication 60404-6 Edition 2, Part 6: Methods of measurement of the magnetic properties of magnetically soft metallic and powder materials at frequencies in the range 20 Hz to 200 kHz by the use of ring specimens, 2003-06, Geneva, IEC Central Office.

[27] S. Zurek, A. J. Moses, M. Packianather, P. Anderson, and F. Anayi, "Prediction of power loss and permeability with the use of an artificial neural network in wound toroidal cores," *Journal of Magnetism and Magnetic Materials*, vol. 320, no. 20, pp. e1001-e1005, 2008.

[28] L. Brugel, P. Brissonneau, A. Kedous, and J. C. Perrier, "Effects of the Epstein Frame imperfections on the accuracy of power measurements at medium frequencies," *Journal of Magnetism and Magnetic Materials*, vol. 41, no. 1-3, pp. 230-232, 1984.

[29] P. Marketos, S. Zurek, and A. J. Moses, "A method for defining the mean path length of the Epstein frame," *IEEE Transactions on Magnetics*, vol. 43, no. 6, pp. 2755-2757, 2007.

[30] K. Qingyi et al., "Determination of the weighted mean path length of the Epstein frame," *COMPEL: The International Journal for Computation and Mathematics in Electrical and Electronic Engineering*, vol. 33, no. 1-2, pp. 224-233, 2013.

[31] E. Antonelli, E. Cardelli, and A. Faba, "Epstein frame: How and when it can be really representative about the magnetic behavior of laminated magnetic steels," *IEEE Transactions on Magnetics*, vol. 41, no. 5, pp. 1516-1519, 2005.

[32] H. Ahlers and J. D. Sievert, "Comparison of a single strip tester and Epstein frame measurements," *Journal of Magnetism and Magnetic Materials*, vol. 26, no. 3, pp. 176-178, 1982.

[33] G. Parent, R. Penin, J.P. Lecointe, J.F. Brudny, and T. Belgrand, "Determination of Specific Losses in the Limbs of an Epstein Frame Using a Three Epstein Frame Methodology Applied to Grain Oriented Electrical Steels," *Sensors*, vol. 16, no. 6, p. 826, 2016.

[34] J. Sievert, "The measurement of magnetic properties of electrical sheet steel-survey on methods and situation of standards," *Journal of Magnetism and Magnetic Materials*, vol. 215-216, pp. 647-651, 2000.

[35] P. K. Klimczyk, P. Anderson, A. Moses, and M. Davies, "Influence of cutting techniques on magnetostriction under stress of grain oriented electrical steel," *IEEE Transactions on Magnetics*, vol. 48, no. 4, pp. 1417-1420, 2012.

[36] G. Loisos and A. J. Moses, "Effect of mechanical and Nd: YAG laser cutting on magnetic flux distribution near the cut edge of non-oriented steels," *Journal of Materials Processing Technology*, vol. 161, no. 1, pp. 151-155, 2005.

[37] J. Sievert et al., "New Data on the Epstein to Single Sheet Tester Relationship," *Przeglad Elektrotechniczny*, vol. 7, no. 13, pp. 1-3, 2013.

[38] J. Sievert and H. Ahlers, "Epstein to SST relationship-Statistical rather than deterministic," *Przeglad Elektrotechniczny*, vol. 87, no. 9b, pp. 17-19, 2011.

[39] D. Miyagi, T. Yamazaki, D. Otome, M. Nakano, and N. Takahashi, "Development of measurement system of magnetic properties at high flux density using novel single-sheet tester," *IEEE Transactions on Magnetics*, vol. 45, no. 10, pp. 3889-3892, 2009.

[40] T. Nakata, Y. Ishihara, N. Takahashi, and Y. Kawase, "Analysis of magnetic fields in a single sheet tester using an H coil," *Journal of Magnetism and Magnetic Materials*, vol. 26, no. 1-3, pp. 179-180, 1982.

[41] F. Fiorillo, G. Durin, and L. Rocchino, "A reference system for the measurement of low-strength magnetic flux density," *Journal of Magnetism and Magnetic Materials*, vol. 304, no. 2, pp. e540--e542, 2006.

[42] Y. Guo et al., "Calibration of sensing coils of a three-dimensional magnetic property tester," *IEEE Transactions on Magnetics*, vol. 42, no. 10, pp. 3243-3245, 2006.

[43] C. Svala, "An improved, practical Burrows permeameter," *IEEE Transactions on Magnetics*, vol. 12, no. 6, pp. 816-818, 1976.

[44] J.P. Barranger, "Very high temperature permeameter," *Journal of Applied Physics*, vol. 42, no. 4, pp. 1796-1797, 1971.

[45] A. Nafalski, A.J. Moses, T. Meydan, and M.M. Abousetta, "Loss measurements on amorphous materials using a field-compensated single-strip tester," *IEEE Transactions on Magnetics*, vol. 25, no. 5, pp. 4287-4291, 1989.

[46] F. G. Baily, "The hysteresis of iron and steel in a rotating magnetic field," *Philos. Trans. R. Soc.*, vol. 187, pp. 715–746, 1896.

[47] A. J. Moses, "Importance of rotational losses in rotating machines and transformers," *Journal of Materials Engineering and Performance*, vol. 1, no. 2, pp. 235-244, 1992.

[48] H. Pfutzner et al., "Rotational magnetization in transformer cores: A review," *IEEE Transactions on Magnetics*, vol. 47, no. 11, pp. 4523-4533, 2011.

[49] A. Moses and B. Thomas, "Problems in the design of power transformers," *IEEE Transactions on Magnetics*, vol. 10, no. 2, pp. 148-150, 1974.

[50] A. T. Moghadam and A. J. Moses, "Comparison of flux distribution in three-phase transformer cores assembled from amorphous material and grain oriented silicon iron," *IEEE Transactions on Magnetics*, vol. 25, no. 5, pp. 3964-3966, 1989.

[51] J. Sievert et al., "European intercomparison of measurements of rotational power loss in electrical sheet steel," *Journal of Magnetism and Magnetic Materials*, vol. 160, pp. 115-118, 1996.

[52] C. Ragusa, S. Zurek, C. Appino, and A.J. Moses, "An intercomparison of rotational loss measurements in non-oriented Fe-Si alloys," *Journal of Magnetism and Magnetic Materials*, vol. 320, no. 20, pp. e623-e626, 2008.

[53] N. Nencib, A. Kedous-Lebouc, and B. Cornut, "Performance evaluation of a large rotational single sheet tester," *Journal of Magnetism and Magnetic Materials*, vol. 160, pp. 174-176, 1996.

[54] A. Kaplan, "Magnetic core losses resulting from a rotating flux," *Journal of Applied Physics*, vol. 32, no. 3, pp. 370–371, 1961.

[55] A. Moses and B. Thomas, "Measurement of rotating flux in silicon iron laminations," *IEEE Transactions on Magnetics*, vol. 9, no. 4, pp. 651-654, 1973.

[56] R. D. Strattant and F. J. Young, "Iron losses in elliptically rotating fields," *Journal of Applied Physics*, vol. 33, no. 3, pp. 1285–1286, 1962.

[57] J. Sievert et al., "The measurement of rotational power loss in electrical sheet steel using a vertical yoke system," *Journal of Magnetism and Magnetic Materials*, vol. 112, no. 1-3, pp. 91-94, 1992.

[58] S. Zouzou, A. Kedous-Lebouc, and P. Brissonneau, "Magnetic properties under unidirectional and rotational field," *Journal of Magnetism and Magnetic Materials*, vol. 112, no. 1-3, pp. 106–108, 1992.

[59] A. Basak and A. J. Moses, "Influence of stress on rotational loss in silicon iron," *Proc. Inst. Elect. Eng.*, vol. 125, no. 2, pp. 165–168, 1978.

[60] M. Enokizono and N. Soda, "Direct magnetic loss analysis by FEM considering vector magnetic properties," *IEEE Transactions on Magnetics*, vol. 34, no. 5, pp. 3008-3011, 1998.

[61] J. Xu and J. Sievert, "On the reproducibility, standardization aspects and error sources of the fieldmetric method for the determination of 2D magnetic properties of electrical sheet steel," in *Proceedings of the 5th International Workshop on Two-dimensional Magnetization Problems*, Grenoble, 1997, pp. 43-54.

[62] M. Enokizono and J. D. Sievert, "Numerical analysis of accuracy of rotational magnetic loss measurement apparatus," *IEEE translation journal on Magnetics in Japan*, vol. 5, no. 9, pp. 742-748, 1990.

[63] S. Zurek and T. Meydan, "Digital feedback controlled RSST system," in *Proceedings of the 16th Soft Magnetic Materials conference (SMM'16)*, Düsseldorf, 2003.

[64] J. G. Zhu and V. S. Ramsden, "Measurement and modelling of losses under two dimensional excitation in rotating electrical machines," in *Proceedings of the 5th International Workshop on Two-dimensional Magnetization Problems*, Grenoble, 1997.

[65] C. Ragusa and F. Fiorillo, "A three-phase single sheet tester with digital control of flux loci based on the contraction mapping principle," *Journal of Magnetism and Magnetic Materials*, vol. 304, no. 2, pp. e568-e570, 2006.

[66] S. Zurek, P. Marketos, T. Meydan, and A. J. Moses, "Use of novel adaptive digital feedback for magnetic measurements under controlled magnetizing conditions," *IEEE Transactions on Magnetics*, vol. 41, no. 11, pp. 4242-4249, 2005.

[67] S. Zurek, "Practical implementation of universal digital feedback for characterisation of soft magnetic materials under controlled AC waveforms," *Przeglad Elektrotechniczny (Electrical Review)*, vol. 93, no. 7, pp. 16-21, 2017.

[68] N. Alatawneh and P. Pillay, "Design of a novel test fixture to measure rotational core losses in machine

laminations," *IEEE Transactions on Industry Applications*, vol. 48, no. 5, pp. 1467-1477, 2012.

[69] Y. Li et al., "Study on Rotational Hysteresis and Core Loss Under Three-Dimensional Magnetization," *IEEE Transactions on Magnetics*, vol. 47, no. 10, pp. 3520-3523, 2011.

[70] J. Zhong, Y. Guo, J. Zhu, H. Lu, and J. Jin, "Development of measuring techniques for rotational core losses of soft magnetic materials," *Nature Sciences*, vol. 2, no. 1, pp. 1-12, 2007.

[71] W. Salz, "A two-dimensional measuring equipment for electrical steel," *IEEE Transactions on Magnetics*, vol. 30, no. 3, pp. 1253-1257, 1994.

[72] W. Brix, K. Hempel, and W. Schroeder, "Method for the measurement of rotational power loss and related properties in electrical steel sheets," *IEEE Transactions on Magnetics*, vol. 18, no. 6, pp. 1469-1471, 1982.

[73] H. Pfützner and G. Krismanic, "The needle method for induction tests: sources of error," *IEEE Transactions on Magnetics*, vol. 40, no. 3, pp. 1610-1616, 2004.

[74] V. Gorican, A. Hamler, M. Jesenik, B. Stumberger, and M. Trlep, "Unreliable determination of vector B in 2-D SST," *Journal of Magnetism and Magnetic Materials*, vol. 254-255, pp. 130-132, 2003.

[75] J. Sievert, "Recent advances in the one-and two-dimensional magnetic measurement technique for electrical sheet steel," *IEEE Transactions on Magnetics*, vol. 26, no. 5, pp. 2553-2558, 1990.

[76] J. Sievert, "Studies on the measurement of two dimensional magnetic phenomena in electrical sheet steel at PTB," *PTB-Bericht*, vol. 43, pp. 102-116, 1992.

[77] S. Zurek, "Effect of off-axis H-coil sensitivity on clockwise–anticlockwise differences of rotational power loss in isotropic samples," *IET Science, Measurement & Technology*, 2018, DOI: 10.1049/iet-smt.2017.0385.

[78] S. Zurek and T. Meydan, "On the difference between clockwise and anticlockwise power losses, Part 1: Mathematical study," *IEE Proceedings, Science, Measurement & Technology*, vol. 153, no. 4, pp. 147–151, 2006.

[79] T. Todaka, Y. Maeda, and M. Enokizano, "Counterclockwise/clockwise (CCW/CW) rotational losses under high magnetic field," *Przeglad Elektrotechniczny*, vol. 85, no. 1, pp. 20-24, 2009.

[80] S. Zurek and T. Meydan, "On the difference between clockwise and anticlockwise power losses, Part 2: Physical phenomena," *IEE Proceedings, Science, Measurement & Technology*, vol. 153, no. 4, pp. 152-157, 2006.

[81] R.S. Albir and A.J. Moses, "Improved dc bridge method employed to measure local power loss in electrical steels and amorphous materials," *Journal of Magnetism and Magnetic Materials*, vol. 83, no. 1-3, pp. 553-554, 1990.

[82] S. Zurek and T. Meydan, "Rotational power losses and vector loci under controlled high flux density and magnetic field in electrical steel sheets," *IEEE transactions on magnetics*, vol. 42, no. 10, pp. 2815-2817, 2006.

[83] S. Spornic, D. Moussaoui, A. Kedous-Lebouc, and B. Cornut, "Frequency magnetic behaviour of SiFe sheets in a rotational field," *Journal of magnetism and magnetic materials*, vol. 160, pp. 147-148, 1996.

[84] A. Kedous-Lebouc, C. Vernescu, and B. Cornut, "A two-dimensional Preisach particle for vectorial hysteresis modeling," *Journal of magnetism and magnetic materials*, vol. 254, pp. 321-323, 2003.

[85] Y. Maeda, T. Todaka, H. Shimoji, M. Enokizono, and J. Sievert, "An evaluation method of cross-type H-coil angle for accurate two-dimensional vector magnetic measurement," *Journal of Magnetism and Magnetic Materials*, vol. 304, no. 2, pp. 564-567, 2006.

[86] K. Mori, S. Yanase, Y. Okazaki, and S. Hashi, "2-D magnetic rotational loss of electrical steel at high magnetic flux density," *IEEE transactions on Magnetics*, vol. 41, no. 10, pp. 3310-3312, 2005.

[87] E. Sulaiman, T. Kosaka, Y. Tsujimori, and N. Matsui, "Design of 12-slot 10-pole Permanant Magnet Flux-Switching Machine with hybrid excitation for hybrid electric vehicle," in *Power Electronics, Machines and Drives Conference (PEMD)* , 2010.

[88] O. de la Barrière et al., "A novel magnetizer for 2D broadband characterization of steel sheets and soft magnetic composites," *International Journal of Applied Electromagnetics and Mechanics*, vol. 48, pp. 239–245, 2015.

[89] C. Appino, O. de la Barriere, C. Beatrice, F. Fiorillo, and C. Ragusa, "Rotational magnetic losses in non-oriented Fe-Si and Fe-Co laminations up to the kHz range," *IEEE Transactions on Magnetics*, vol. 50, no. 11, pp. 1-4, 2014.

[90] C. Appino et al., "Skin effect in steel sheets under rotating induction," *International Journal of Applied Electromagnetics and Mechanics*, vol. 48, pp. 247-254, 2015.

[91] Y. Li et al., "Measurement of Soft Magnetic Composite Material Using an Improved 3-D Tester With Flexible Excitation Coils and Novel Sensing Coils," *IEEE Transactions on Magnetics*, vol. 46, no. 6, pp. 1971-1974, 2010.